Korean J. Chem. Eng., 40(5), 1063-1070 (2023)
DOI: 10.1007/s11814-022-1301-2

pISSN: 0256-1115
eISSN: 1975-7220

Optimization of water-saturated superabsorbent polymers for hydrate-based gas storage

Min-Kyung Kim*,‡, Geumbi Han*,‡, Hyeonjin Kim*, Jihee Yu*, Youngki Lee*, Taekyong Song, Jinmo Park**, Yo-Han Kim**, and Yun-Ho Ahn*,†**

*Department of Chemical Engineering, Soongsil University, 369 Sangdo-ro, Dongjak-gu, Seoul 06978, Korea
**Hydrogen Research Center, KOGAS Research Institute, 960 Incheonsinhangdaero, Yeonsu-gu, Incheon 21993, Korea
(*Received 12 August 2022 • Revised 18 September 2022 • Accepted 25 September 2022*)

Abstract−Gas hydrates are an environmentally benign and cost-effective gas storage media that can store gas molecules in a lattice formed by hydrogen bonds between water molecules. To utilize gas hydrates on an industrial scale, the formation rate of gas hydrates must be improved. In this study, superabsorbent polymer (SAP) having a three-dimensional porous polymeric network was used to promote the formation of natural gas hydrates. SAP can absorb water efficiently and improve the kinetics of natural gas hydrates without mechanical agitation by expanding the gas-water interfacial area. The promotion effect of SAP is affected by various factors: the formation rate of natural gas hydrate and its reproducibility are determined by how water is dispersed over the SAP powders. Moreover, as the SAP is less crosslinked, the natural gas hydrate formation occurs more rapidly. The amount of saturated water is also a critical factor in determining the formation rate and yield of natural gas hydrates. Through this study, we provide engineering data to design hydrate-based gas storage media in a quiescent system for a large-scale application.

Keywords: Clathrate Hydrates, Natural Gas Hydrate, Natural Gas Storage, Superabsorbent Polymer, Water-saturation Strategy

INTRODUCTION

The continuous emission of greenhouse gases from the combustion of conventional fossil fuels has accelerated global warming and other aspects of environmental damage [1]. Natural gas, which is primarily composed of 90 percent or more methane balanced with small portions of ethane, propane, and butane, has been recognized as the cleanest-burning hydrocarbon among carbon-based fuels because it generates less carbon dioxide (up to 50 percent emission compared to oils or coals) and harmful air pollutants (such as nitrogen oxide, sulfur oxide, etc.) along with combustion [2]. In 2040, natural gas is anticipated to account for 203 trillion cubic feet (Tcf), constituting 22 percent of the world's energy sources. As the demand for natural gas keeps rising, we must develop storage and transport solutions that are ecological and energy-efficient [3].

Two types of natural gas are commercially available: liquefied natural gas (LNG) and compressed natural gas (CNG) [4,5]. Low temperatures of around 110 K and a sophisticated production procedure are often required to liquefy natural gas. Since CNG does not require such a low temperature, it is commonly utilized in vehicles. However, CNG must be stored at high pressure (~25 MPa) in a vessel designed specifically for high-pressure storage. To overcome these disadvantages, substantial research has been conducted on solidified natural gas (SNG) [6]. This study focuses on clathrate hydrate-based natural gas storage, one of the SNGs, for the safe and environmentally friendly storage of natural gas.

Clathrate hydrates, commonly known as gas hydrates, are crystalline compounds capable of storing energy carriers within a lattice created by hydrogen bonds between water molecules [7]. Because gas hydrates are composed of water and can store natural gas under milder conditions than LNG or CNG, hydrate-based gas storage is environmentally benign and energy-efficient. Moreover, gas hydrates are safer than alternative physical-based gas storage media since they do not explode. However, due to drawbacks in formation kinetics and thermodynamics, gas hydrates cannot be used on an industrial scale. Overcoming these constraints requires optimizing the formation and dissociation rates of gas hydrate as well as the thermodynamic conditions. Various liquid-phase thermodynamic promoters have been discovered [8-11], and tetrahydrofuran (THF) [12-15] and cyclopentane (CP) [16,17] are the representative promoters that lower a required formation pressure or raise a required formation temperature. Nonetheless, these promoters occupy the large cavities of gas hydrates where gas molecules can be stored, reducing the storage capacity. Gas-phase thermodynamic promoters of energy carriers (*e.g.*, methane and ethane) were also utilized to store hydrogen in the mixed gas hydrates to improve energy density [18,19]. In addition, numerous studies have been conducted to enhance the formation rate of gas hydrates in a quiescent system by developing novel systems [20-22] or expanding the gas-water interface through the use of porous media to achieve "energy efficiency" [16,23-26].

In this study, the formation rates of natural gas hydrates were increased using superabsorbent polymers (SAPs) as porous media. SAP, which absorbs and retains a large quantity of water, consists of a three-dimensional network of hydrophilic polymer chains that are crosslinked and produced by interactions with monomers and crosslinking agents. SAP is reported to absorb liquids 1,000 times

†To whom correspondence should be addressed.
E-mail: yhahn@ssu.ac.kr
‡Min-Kyung Kim and Geumbi Han equally contributed to this work.

its mass or greater [27]. It contains water as the polymer expands due to the capillary force of microporous structures or interactions with functional groups or polymer chains. Kang et al. demonstrated that increasing the gas-water contact area in a water-dispersed SAP system significantly increased the methane hydrate formation rate. In addition, they confirmed that methane could be stored sustainably for 20 cycles of formation-dissociation without energy-intensive mechanical agitation [28]. The water-saturated SAP system was also effective for the carbon dioxide capture [29]. This study aimed to find the best conditions for water saturation in SAP and explore the relationship between the kinetics of natural gas hydrate formation, the degree of crosslinking, and the water content within SAP.

EXPERIMENTAL SECTION

1. Materials

Deionized water of ultrahigh purity was obtained from a Direct-Q3 water purification unit (Millipore, Burlington, USA, resistivity >18.2 MΩ·cm). The simulated natural gas consisting of CH_4+C_2H_6+C_3H_8 was purchased from Seoul Specialty Gas Co. (Republic of Korea). The composition of the synthetic natural gas used in the experiment was CH_4 (90.0 mol%)+C_2H_6 (7.0 mol%)+C_3H_8 (3.0 mol%). Super-absorbent polymer (SAP, sodium polyacrylate), having particle size less than 1,000 μm, was supplied by Jeije Co. (Republic of Korea). This study used two different types of SAPs: highly crosslinked SAP (HCS) and low crosslinked SAP (LCS). SAPs were dried overnight in the vacuum oven at 323 K and used without further treatment.

2. Formation of Natural Gas Hydrates within SAP

To find optimal water content for the rapid formation of natural gas hydrate within SAP, we varied the water-to-SAP ratio that could present water-absorbing capacity of SAP. The "water-to-SAP ratio" (WSR) could be defined as follows:

$$\mathrm{WSR} = \frac{\text{mass of water (g)}}{\text{mass of SAP (g)}}$$

The volume of water was held constant at 30 mL, while the mass of SAP was varied in accordance with WSR. When dispersing water in SAP, it is essential that the water is evenly distributed across all particles. To determine the optimal water-dispersing technique, numerous strategies were tried. The following are the detailed water-dispersing techniques:

Water-dispersing technique 1: After determining the mass of SAP in accordance with WSR, we loaded SAP evenly into the reactor. The 30 mL of water was then injected into the reactor by a syringe maintaining a kind of layer to be dispersed as evenly as possible (described in Fig. 1(a)).

Water-dispersing technique 2: We loaded 30 mL of water and SAP, calculated according to WSR as in Water-dispersing technique 1. But the total amount of water and SAP was divided by five before loading. When one-fifth of SAP and water was sequentially loaded, we waited until the SAPs were fully saturated with water. After that, we repeated additional four processes to inject all the required amount of SAP and water (described in Fig. 1(b)).

Water-dispersing technique 3: We put 30 mL of water on a petri dish and then spread all SAPs at once using a spatula. The fully-

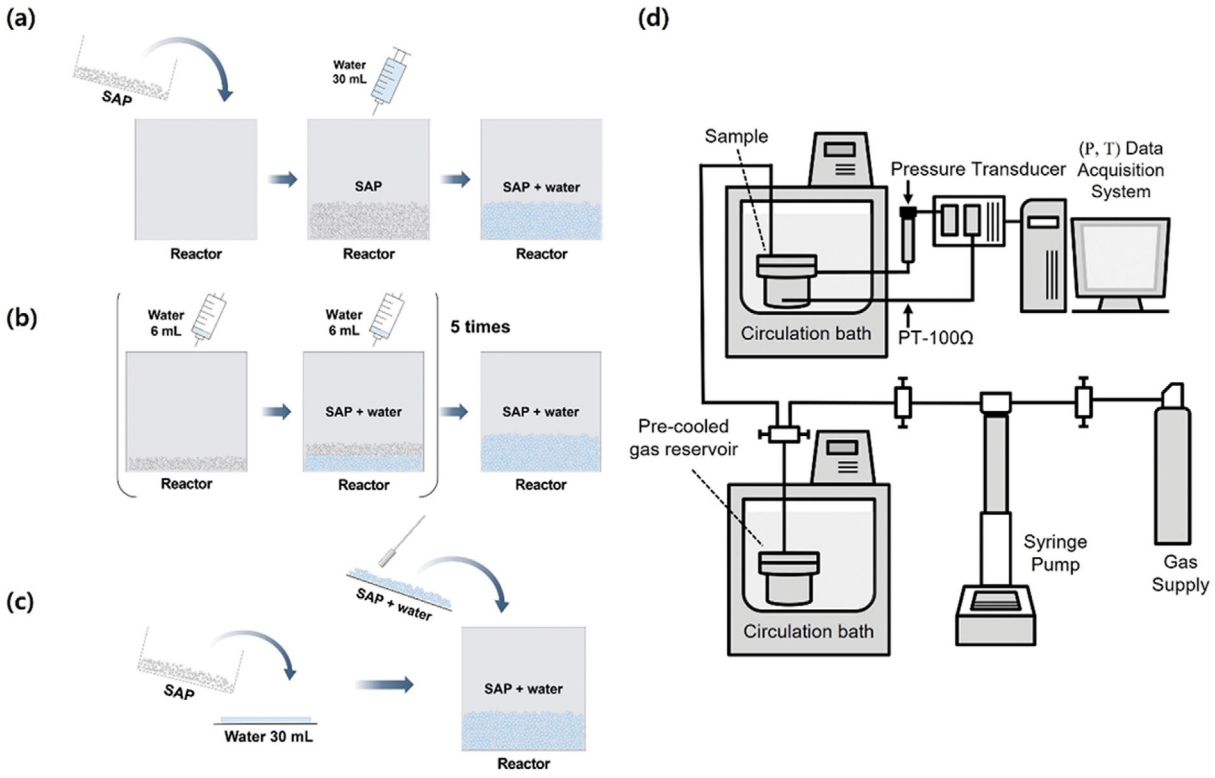

Fig. 1. Schematic diagram of (a) water-dispersing technique 1, (b) water-dispersing technique 2, (c) water-dispersing technique 3, and (d) the overall gas hydrate formation system.

saturated SAPs were transferred into the reactor. We tried to minimize a gap between SAP particles to make them packed as dense as possible (described in Fig. 1(c)).

After three different water-dispersing techniques were used to prepare the water-saturated SAPs in the reactor, the reactor was placed in a refrigerated ethanol circulator (RW3-2025P, Jeio Tech Co., Republic of Korea) at 275 K. When the temperature was stabilized, the water-saturated SAP was pressurized to the desired pressure (3.0 and 4.5 MPa in this study) with pre-cooled natural gas. During the formation of natural gas hydrate, the system pressure and temperature profiles were monitored using a pressure transducer (PSHB0250BCPG, Sensys Co., Republic of Korea, ±0.15% full-scale accuracy, 0-25 MPa) and a four-wire type Pt-100Ω probe (full-scale accuracy of ±0.05%, 13-923 K), respectively. A detail experimental setup is described in Fig. 1(d).

3. Guest Distribution Analysis Using Raman Spectroscopy

Using Raman spectroscopy, the guest-distribution of natural gas hydrates was determined. Before recovering natural gas hydrate samples, the reactor was quenched in a liquid nitrogen to minimize the dissociation of natural gas hydrates. After a few seconds, the reactor was vented, and then natural gas hydrates were recovered and finely ground with a 200 μm sieve under a liquid nitrogen. The Raman spectrum of natural gas hydrates was obtained using a dispersive Raman spectrometer (ARAMIS, Horiba Jobin Yvon Inc., France). The excitation source was a 514.53-nm-long-wavelength Ar ion laser. The scattered light was dispersed by the 1,800 grating of the spectrometer and detected by a charge-coupled device (CCD) with electrical cooling (203 K). The temperature of the sample was maintained at 93 K using a THMSG 600 unit (Linkam Scientific, United Kingdom).

4. Kinetic Analysis of Natural Gas Hydrates within SAPs

To investigate the kinetic performance of certain systems, some researchers have measured the induction time [30,31]. In this study, however, we were unable to determine the induction time because the natural gas hydrates were formed concurrently within the water-saturated SAPs under natural gas pressure. Consequently, t_{rapid} was utilized to analyze the formation rate of natural gas hydrates within SAPs, as reported by Kang et al. [28] t_{rapid} was defined as the period until the pressure decrement over time (dP/dt) reaches 0.001, resulting in a gradient of pressure profile that is almost constant. The pressure difference (ΔP) between the initial pressure ($P_{initial}$) and the pressure at t_{rapid} (P_{rapid}) can be calculated as $\Delta P=P_{initial}-P_{rapid}$. For clear comparison, we normalized the pressure difference by the initial pressure as follows: $\Delta P_{norm}=\Delta P/P_{initial}$.

5. Storage Capacity of Natural Gas Hydrates

To determine the storage capacity of natural gas hydrates, we adopted the water displacement method (Fig. S1) [32]. A portion of the recovered natural gas hydrate samples from the synthesis reactor was transferred to a second pre-cooled reactor for complete dissociation. The reactor was linked to the mass cylinder to collect all of the natural gas coming from the dissociated natural gas hydrates. The amount of stored gas (V_{gas}) could be directly measured. As we knew the weight of water-saturated SAPs and the WSR value, the natural gas storage capacity of V_{gas}/V_{water} could be easily obtained.

RESULTS AND DISCUSSION

1. Guest Distribution in the Natural Gas Hydrates

For guest distribution investigation of natural gas hydrates, Raman spectra were measured. Here we note that the Raman spectrum depicted in Fig. 2 is the average of three spectra obtained from various locations on the surface of the natural gas hydrates. C_2H_6 and C_3H_8 were stored in the large cavities ($5^{12}6^4$ cages) of structure II (sII) hydrates, as shown by the peaks at 876 and 990 cm^{-1}, which correspond to C-C stretching modes of C_2H_6 and C_3H_8 molecules [7,33]. The enclathration of C_2H_6 and C_3H_8 in sII-L cavities could also be cross-checked using the C-H stretching modes: two peaks at 2,868 and 2,876 cm^{-1} correspond to the C-H stretching modes of C_3H_8, while two peaks at 2,884 and 2,939 cm^{-1} correspond to those of C_2H_6 [34]. In contrast to C_2H_6 and C_3H_8 molecules, smaller CH_4 molecules can be stored in both the large

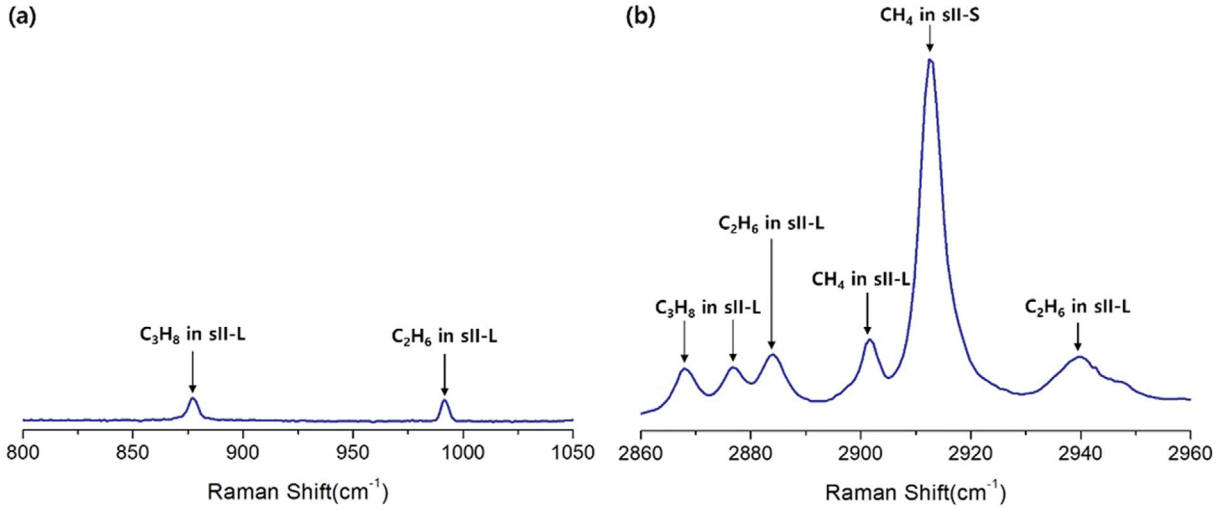

Fig. 2. Guest distribution of mixed gas (CH_4 90%+C_2H_6 7%+C_3H_8 3%) hydrates. (a) C-C vibron region in Raman spectrum for C_2H_6 and C_3H_8 in sII large cages (b) C-H vibron region in Raman spectrum for CH_4, C_2H_6, and C_3H_8 in sII large cages and CH_4 in sII small cages.

and small cavities of sII hydrates: the peaks at 2,901 and 2,911 cm^{-1} correspond to the C-H stretching modes of CH_4 in sII-L and sII-S, respectively [33,35]. The unit cell of sII hydrates consists of eight large cavities and sixteen small cavities ($8(5^{12}6^4)\cdot16(5^{12})\cdot136H_2O$) [36]. Considering that all natural gas components can be stored in sII-L cavities but only CH_4 can be stored in sII-S cavities, the intensity of the peak at 2,911 cm^{-1} is significantly larger than that of other peaks. These Raman results are similar to other natural gas hydrates formed in a bulk, pure water phase, implying that the SAPs just acted as a physical support that did not affect the cage occupation behavior of each component of natural gas.

2. Effects of Water-dispersing Technique on Natural Gas Hydrate Formation

The formation characteristics of natural gas hydrate in a quiescent system must be explored systematically to develop a large-scale, energy-efficient hydrate-based natural gas storage system. If we attempt to thoroughly saturate a huge quantity of SAPs with water, the SAPs must be heterogeneous, with differing water content in the inner and exterior parts of the bulk SAPs. Moreover, concentrated water at the exterior part of the water-absorbed SAPs may hinder the mass transfer of the natural gas to the interior part, resulting in a reduction in natural gas storage capacity and a decrease in the formation rate of natural gas hydrates. Therefore, we need to optimize the water-saturation technique to produce SAPs that are uniformly water-saturated for large-scale applications.

Initially, water-saturated SAPs prepared using the water-dispersing technique 1 (described in section 2.2 and Fig. 1(a)) were analyzed. As the bulk water was rapidly introduced to the aggregated SAP powders, the upper part of the SAPs absorbed a large amount of water first, forming a mass-transfer resistant barrier composed of immobilized water that may inhibit the diffusion of water inside the SAP powders. Thus, water may not be distributed homogeneously. As we expected, even though we used SAP as a water-dispersing matrix, the induction time for the fourth trial with a WSR value of 9 was around 70 minutes (Fig. 3(a)). The induction times were also observed with the WSR values of 6 and 7, and these induction times were not similar in two independent trials, indicating that water-dispersing technique 1 is incapable of producing reproducible water-saturated SAPs for the rapid nucleation and growth of natural gas hydrates (Fig. S2). In addition, we also varied the WSR value from 9 to 36, and we examined each WSR value five times for the kinetic performance study (Fig. 3(b)). The t_{rapid} values were not identical or comparable for the same WSR value showing relatively large error bars: the direct injection of bulk water into the aggregated SAP powders (water-dispersing technique 1) is not the preferable procedure for the reproducible and rapid formation of natural gas hydrates. Here we note that arbitrary WSR values were adopted in this section to investigate the effects of water-dispersing technique on the formation of natural gas hydrate, and the optimization of WSR values will be discussed in the section 3.4.

The aforementioned result may be affected by the geometry of the reactor or the packing density of the SAP powders. If the diameter is much lower than the height, the surface area of aggregated SAP powders exposed to the injected water should be limited. Also, if the SAP powders are packed densely when they are placed into the reactor, water cannot diffuse to the bottom of the reactor. To minimize these expected variables, we implemented the water-dispersing technique S1 shown in Fig. S3(a): On the PVC cling film, we spread SAP powders as thinly as possible and sprinkled the same quantity of water as in the water-dispersing technique 1. To prevent SAP loss during sample loading, the cling film containing water-saturated SAPs was then transferred to the reactor. Although we confirmed that SAP powders were uniformly saturated with water prior to reactor loading, induction times with arbitrary WSR values of 15 and 30 were observed (Fig. S4). We hypothesized that the cling film and the space between cling film and the reactor acted as heat-transfer barrier, resulting in delayed thermal equilibrium with the surroundings or slow heat release during the exothermic nucleation and growth of natural gas hydrates, as there was no induction time in the SAPs prepared by the water-dispersing technique 1 with the same WSR values of 15 and 30 (Fig. S4).

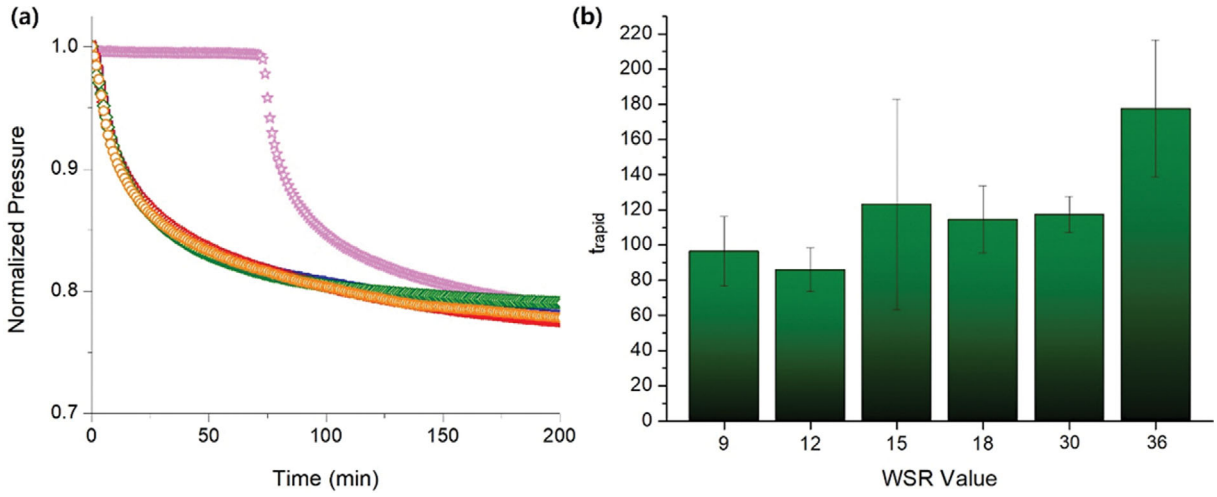

Fig. 3. (a) Pressure changes of trials 1-5 for water-dispersing technique 1 with WSR value of 9 (◁, trial 1; ◇, trial 2; □, trial 3; ☆, trial 4; ○, trial 5) (b) Measured t_{rapid} for various WSR values.

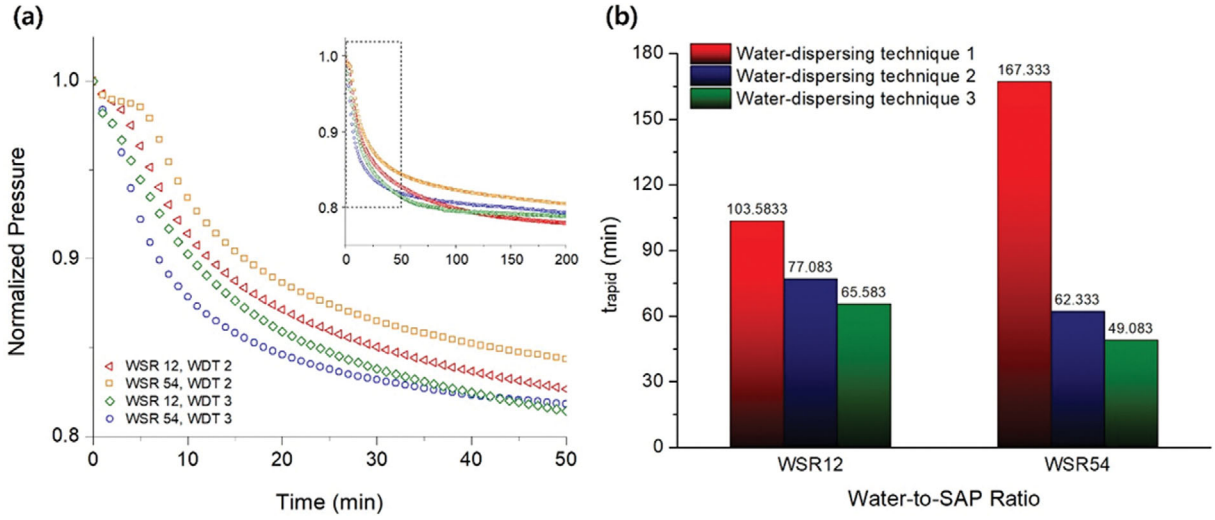

Fig. 4. (a) Pressure changes with $P_{initial}$ of 30 bar for different water-dispersing techniques (WDT) and WSR values (◁, WSR 12, water-dispersing technique 2 (WDT 2); □, WSR 54, water-dispersing technique 2 (WDT 2); ◇, WSR 12, water-dispersing technique 3 (WDT 3); ○, WSR 54, water-dispersing technique 3 (WDT 3)). (b) The values of t_{rapid} with the WSR values of 12 and 54 using different water-dispersing techniques.

We attempted to introduce water using water-dispersing technique 2 described in Fig. 1(b) to improve heat transfer and achieve thermal equilibrium more quickly. Small amounts of SAP powders and water were sequentially injected into the reactor, and this process was continued until the desired amount of SAP powders and water was attained. At each step, sufficient time was allowed for the water-saturation reaction to reach equilibrium. In addition, as the water-saturated SAPs were prepared inside the reactor, the gap between the SAPs and the reactor might be minimized improving heat transfer between system and surroundings. Simultaneously, water-dispersing technique 3 described in Fig. 1(c) was also employed for another system; this approach was similar to the technique S1, except that the cling was not loaded into the reactor. Using both water-dispersing techniques 2 and 3, the WSR values were 12 and 54, and the normalized pressure changes and t_{rapid} values are presented in Fig. 4(a) and (b), respectively. The normalized pressure change patterns during the formation of natural gas hydrates did not significantly differ in the two different water-dispersing techniques. However, the normalized pressures for both WSR values during the initial 50 minutes were somewhat lower for water-dispersing technique 3 than for water-dispersing technique 2 (Fig. 4(a)), suggesting that more natural gas was stored in the hydrate media when the water-saturated SAPs were prepared via water-dispersing technique 3. Comparing the t_{rapid} values for the WSR values of 12 and 54, we could observe the smallest t_{rapid} values in water-dispersing technique 3 (65.583 min and 49.083 min, respectively) (Fig. 4(b)). This indicates that water-dispersing technique 3 showed the best performance in terms of formation rate of natural gas hydrates (Fig. 4(b) and Table S1) and overall formation yield of natural gas hydrates (Fig. 4(a)).

Lastly, we slowly dropped SAPs particle-by-particle into the water-filled reactor (Technique S2 described in Fig. S3(b)). Despite the fact that all SAPs were LCS with the same WSR value of 12, only the SAP prepared by technique S2 showed the induction time (Fig. S5). Therefore, we could conclude that water dispersion of SAP powders should be performed outside the reactor (water-dispersing technique 3) rather than inside the reactor (water-dispersing technique 1, 2, and S2).

3. Effects of Crosslinking on Natural Gas Hydrate Formation

Two kinds of SAPs having different degrees of crosslinking were prepared to explore the effect of crosslinking on the natural gas hydrate formation. In general, the degree of crosslinking can be controlled by varying the amount of crosslinking agent, and the water-absorbing capability of crosslinked SAP is inversely proportional to the degree of crosslinking: highly crosslinked SAP absorbs less water; however, its physical properties (*e.g.*, gel strength) become more strengthened. In this work, highly crosslinked SAP (HCS)

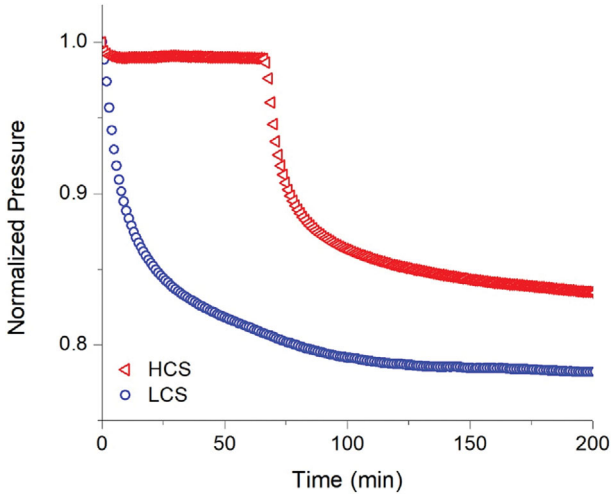

Fig. 5. Pressure changes during the formation of natural gas hydrates within HCS and LCS prepared by water-dispersing technique 3 at 30 bar, with the WSR value of 30 (◁, HCS (Highly crosslinked SAP); ○, LCS (Low crosslinked SAP)).

Table 1. Kinetic performances for the systems having with the WSR value of 30 and two different degrees of crosslinking in water-dispersing technique 3 at 30 bar

Type of SAP	t_{rapid} [min][a]	$P_{initial}$ [bar]	ΔP [bar][b]	ΔP_{norm} [b]
LCS	83.08	29.97	6.064	0.2024
HCS	118.50[a]	30.64	4.516	0.1474

[a]The t_{rapid} for HCS was the duration time including the induction time. Induction time was 66.92 min.
[b]Time interval of ΔP, ΔP_{norm} was 0~t_{rapid} min.

and low crosslinked SAP (LCS) were used as a water-saturated platform for a rapid formation of natural gas hydrate. LCS has a lower degree of crosslinking but a higher water-absorbing capability than HCS.

Both LCS and HCS were prepared by water-dispersing technique 3 with the identical WSR value of 30, and the pressure change characteristics caused by the formation of natural gas hydrates in LCS and HCS were compared (Fig. 5 and Table 1). For the LCS, the normalized pressure dropped drastically, but after a certain period of time, the change became monotonic. For the HCS, we could observe the induction time (66.92 minutes), and ΔP_{norm} was very small (less than 0.01) during the induction time because the enclathration of natural gas was not initiated at this stage. However, once the nucleation of natural gas hydrate was initiated, the normalized pressure decreased showing much steeper slope than that of the LCS. In addition, the final ΔP_{norm} value for LCS was higher than that for HCS. Thus, we can conclude that LCS is more effective in terms of formation rate and total storage capacity of natural gas hydrates: the SAP should be less crosslinked for the quiescent (*i.e.*, non-stirred, static system) scaled-up process of natural gas storage in the clathrate hydrate medium.

4. Optimal WSR Value for Enhanced Natural Gas Hydrate Formation

In the previous two chapters, we determined that water-dispersing technique 3 was better than other dispersing strategies in terms of the formation rate of natural gas hydrates. Moreover, we found that the LCS functioned better than the HCS: more natural gas hydrates could be formed more quickly in the LCS. As a last optimization step, we analyzed the impact of water content in SAPs on the formation rate and overall yield of natural gas hydrates.

Using water-dispersing technique 3, five types of LCSs having different WSR values (30, 36, 42, 48, and 54) were prepared. The ΔP_{norm} during the natural gas hydrate formation and the summary of a kinetic study are presented in Fig. 6 and Table 2, respectively. As the WSR value increased from 30 to 42, t_{rapid} values increased, implying that natural gas hydrates were formed more slowly at higher water content in SAP matrix. Reversely, from the WSR value of 42 to 54, the values of t_{rapid} decreased. Based on these trends, we may misleadingly conclude that the SAP should contain less water (WSR ~ 30) or more water (WSR ~ 54) to promote the formation of natural gas hydrate within the water-saturated SAPs. At this stage, we need to consider ΔP_{norm}: low ΔP_{norm} values indicate that the pressure drop induced by the formation of natural gas hydrates was not considerably greater for the systems with the WSR values of 30 and 54. To optimize both the formation rate and storage

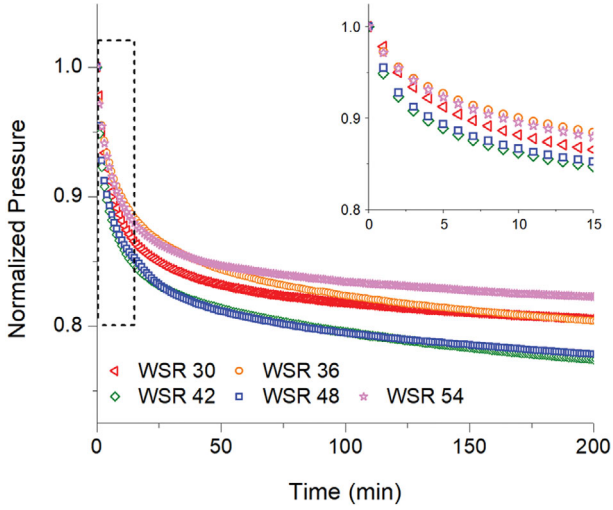

Fig. 6. Pressure changes for various LCS systems with WSR values from 30 to 54 prepared by water-dispersing technique at 45 bar (◁, WSR 30; ○, WSR 36; ◇, WSR 42; □, WSR 48; ☆, WSR 54).

Table 2. Kinetic performance in water-dispersing technique 3 depending on the values of WSR at 45 bar

WSR	t_{rapid} [min]	$P_{initial}$ [bar]	ΔP [bar][a]	ΔP_{norm} [a]
30	77.583	44.89	7.973	0.1776
36	79.083	42.66	7.250	0.1700
42	95.583	45.34	9.229	0.2035
48	85.083	42.54	8.575	0.2016
54	73.583	47.58	7.623	0.1602

[a]Time interval of ΔP, ΔP_{norm} was 0~t_{rapid} min.

capacity of natural gas hydrates, the best WSR value must be selected from the trade-off between t_{rapid} and ΔP_{norm}. The t_{rapid} value was around 85 minutes at the WSR value of 48, which was between WSR values of 42 and 54. However, the value of ΔP_{norm} at WSR 48 was 0.2016, which was near to the maximum value at WSR 42. Based on these data, we concluded that the ideal water-to-SAP ratio at the 30 mL water scale was a WSR value of 48. Here we note that the WSR value interval was just 6. If additional water-saturated SAP samples were prepared with the smaller WSR interval, the WSR value could be accurately optimized. In addition, on a larger scale of water, the WSR value should be optimized with careful consideration for both the formation rate and storage capacity of natural gas hydrates.

Finally, the natural gas storage capacity of hydrates formed in water-saturated SAPs was quantitatively analyzed via water displacement method described in section 2.5. We loaded water with [37] the WSR value of 48 into the LCS using water-dispersing technique 3. The natural gas hydrates were formed at 275 K and 45 bar conditions, and then recovered samples were completely dissociated for measuring the total amount of natural gas stored in hydrate phase. We tried six times, and the results are presented in Table 3. The average storage capacity was 132.15 (V_{gas}/V_{water}) with the standard deviation of 15.95, and this storage capacity was close to the

Table 3. V_{gas}/V_{water} of natural gas hydrates within SAP at WSR 48

No.	Pressure (bar)	Temperature (K)	V_{gas}/V_{water} (v/v (water))	Average of V_{gas}/V_{water} (Standard deviation) (v/v (water))	V_{gas}/V_{water} of reference (v/v (water))[a]
1	44.94	276.27	113.88	132.15 (15.95)	154
2	44.94	276.27	152.84		
3	44.26	276.58	130.34		
4	44.61	276.59	151.60		
5	44.61	276.59	131.66		
6	44.90	276.53	112.60		

[a]The gas composition of reference was $CH_4/C_2H_6/C_3H_8$ (92.05%/4.96%/2.99%). 300 ppm of SDS (Sodium Dodecyl Sulfate) was used to form gas hydrates for 500 min at 45.4 bar, 275.15 K in stirred system [38].

reported values [38].

CONCLUSION

The effects of SAP on the formation of natural gas hydrates were systematically investigated in this study. The formation rate and formation amount of natural gas hydrate in a quiescent system are influenced by the way of water dispersion in the SAPs, the degree of crosslinking, and the water-to-SAP ratios. The water-saturated SAPs just serve as a physical matrix for natural gas hydrate, since the cage occupation behavior of methane, ethane, and propane did not differ significantly from that of natural gas hydrate generated in bulk water. Without mechanical agitation, the SAPs just accelerated the nucleation and growth of natural gas hydrate. When we dispersed water in SAPs outside of the reactor and transferred them inside the reactor (water-dispersing technique 3), the overall kinetic performance and quantity of natural gas hydrates was improved. In addition, SAPs should be less crosslinked for enhanced performance in the formation of natural gas hydrate. In terms of the formation rate and conversion of natural gas hydrate, the optimal water-to-SAP ratio for a constant 30 mL water volume was 48 : 1. Through this study, we believe we have provided a guidance on how to prepare a water-saturated SAP platform for the practical and energy-efficient hydrate-based storage of natural gas at an industrial scale.

ACKNOWLEDGEMENTS

This work was supported by the National Research Foundation of Korea (NRF) grant funded by the Korea government (MSIT) (No. 2021R1F1A1047108). This work was supported by the ERC Center funded by the National Research Foundation of Korea (NRF-2022R1A5A1033719). The authors also acknowledge the financial support from Korea Gas Corporation(KOGAS) under Award No. 2021-02 (202122671542)

AUTHOR CONTRIBUTIONS

†Min-Kyung Kim and Geumbi Han equally contributed to this work.

All authors have approved the final version of the manuscript.

NOTES

The authors declare no competing financial interest.

SUPPORTING INFORMATION

Additional information as noted in the text. This information is available via the Internet at http://www.springer.com/chemistry/journal/11814.

REFERENCES

1. F. Sévellec and S. S. Drijfhout, *Nat. Commun.*, **9**, 1 (2018).
2. U. Epa, C. Change Division, Inventory of U.S. Greenhouse Gas Emissions and Sinks: 1990-2020 – Main Text, 1990. https://www.epa.gov/ghgemissions/draft-inventory-us-greenhouse-gas-emissions (accessed July 11, 2022).
3. J. Conti, P. Holtberg, J. Diefenderfer, A. LaRose, J. T. Turnure and L. Westfall, International Energy Outlook 2016 With Projections to 2040, 2016.
4. J. Kim, Y. Noh and D. Chang, *Appl. Energy*, **212**, 1417 (2018).
5. K. B. Deshpande, W. B. Zimmerman, M. T. Tennant, M. B. Webster and M. W. Lukaszewski, *Chem. Eng. J.*, **170**, 44 (2011).
6. H. P. Veluswamy, A. Kumar, Y. Seo, J. D. Lee and P. Linga, *Appl. Energy*, **216**, 262 (2018).
7. E. D. Sloan and C. A. Koh, *Clathrate hydrates of natural gases*, 3rd Ed., CRC Press (Taylor and Francis Group) (2008).
8. G. Bhattacharjee, M. N. Goh, S. E. K. Arumuganainar, Y. Zhang and P. Linga, *Energy Environ. Sci.*, **13**, 4946 (2020).
9. Y. H. Ahn, Y. Youn, M. Cha and H. Lee, *RSC Adv.*, **7**, 12359 (2017).
10. Y. H. Ahn, H. Kang, M. Cha, K. Shin and H. Lee, *ACS Omega*, **2**, 1601 (2017).
11. H. Kang, Y.-H. Ahn, D.-Y. Koh and H. Lee, *Korean J. Chem. Eng.*, **33**, 1897 (2016).
12. K. Inkong, P. Rangsunvigit, S. Kulprathipanja and P. Linga, *Fuel*, **255**, 115705 (2019).
13. G. Pandey, H. P. Veluswamy, J. Sangwai and P. Linga, *Energy Fuels*, **33**, 4865 (2019).
14. D. W. Kang, W. Lee, Y. H. Ahn and J. W. Lee, *J. Mol. Liq.*, **349**, 118490 (2022).

15. W. Lee, D. W. Kang, Y.-H. Ahn and J. W. Lee, *ACS Sustain. Chem. Eng.*, **9**, 8414 (2021).
16. B. H. Shi, L. Yang, S. S. Fan and X. Lou, *Fuel*, **194**, 395 (2017).
17. S. Baek, Y. H. Ahn, J. Zhang, J. Min, H. Lee and J. W. Lee, *Appl. Energy*, **202**, 32 (2017).
18. Y. H. Ahn, S. Moon, D. Y. Koh, S. Hong, H. Lee, J. W. Lee and Y. Park, *Energy Storage Mater.*, **24**, 655 (2020).
19. S. Moon, Y. Lee, D. Seo, S. Lee, S. Hong, Y. H. Ahn and Y. Park, *Renew. Sustain. Energy Rev.*, **141**, 110789 (2021).
20. H. Kang, Y. H. Ahn, D. Y. Koh, S. Baek, J. W. Lee and H. Lee, *Ind. Eng. Chem. Res.*, **55**, 6079 (2016).
21. S. Baek, J. Min, Y. H. Ahn, M. Cha and J. W. Lee, *Energy Fuels*, **33**, 523 (2019).
22. S. Baek, W. Lee, J. Min, Y. H. Ahn, D. W. Kang and J. W. Lee, *Korean J. Chem. Eng.*, **37**, 341 (2020).
23. V. D. Chari, D. V. S. G. K. Sharma, P. S. R. Prasad and S. R. Murthy, *J. Nat. Gas Sci. Eng.*, **11**, 7 (2013).
24. H. P. Veluswamy, P. S. R. Prasad and P. Linga, *Korean J. Chem. Eng.*, **33**, 2050 (2016).
25. S. Rungrussamee, K. Inkong, S. Kulprathipanja and P. Rangsunvigit, *Chem. Eng. Trans.*, **70**, 1519 (2018).
26. F. Su, C. L. Bray, B. O. Carter, G. Overend, C. Cropper, J. A. Iggo, Y. Z. Khimyak, A. M. Fogg and A. I. Cooper, *Adv. Mater.*, **21**, 2382 (2009).
27. M. J. Zohuriaan-Mehr and K. Kabiri, *Iran. Polym. J.* (English Ed.), **17**, 451 (2008).
28. D. W. Kang, W. Lee, Y. H. Ahn and J. W. Lee, *Chem. Eng. J.*, **411**, 128512 (2021).
29. D. W. Kang, W. Lee and Y. H. Ahn, *J. CO2 Util.*, **61**, 102005 (2022).
30. H. Kim, Y. H. Ahn, Y. Seo and C. D. Wood, *Fuel*, **257**, 116035 (2019).
31. Y. Lee, S. Moon, S. Hong, S. Lee and Y. Park, *Chem. Eng. J.*, **389**, 123749 (2020).
32. F. Inomata, K. Takabe and H. Saiki, *J. Electron Microsc.* (Tokyo), **41**, 369 (1992).
33. H. S. Truong-Lam, H. S. Truong-Lam, S. D. Seo, S. Kim, Y. Seo and J. D. Lee, *Energy Fuels*, **34**, 6288 (2020).
34. S. Subramanian, R. A. Kini, S. F. Dec and E. D. Sloan, *Chem. Eng. Sci.*, **55**, 1981 (2000).
35. R. Kumar, P. Linga, I. Moudrakovski, J. A. Ripmeester and P. Englezos, *AIChE J.*, **54**, 2132 (2008).
36. A. Hassanpouryouzband, E. Joonaki, M. Vasheghani Farahani, S. Takeya, C. Ruppel, J. Yang, N. J. English, J. M. Schicks, K. Edlmann, H. Mehrabian, Z. M. Aman and B. Tohidi, *Chem. Soc. Rev.*, **49**, 5225 (2020).
37. W. Liu, S. Wang, M. Yang, Y. Song, S. Wang and J. Zhao, *J. Nat. Gas Sci. Eng.*, **24**, 357 (2015).
38. Z. G. Sun, R. Wang, R. Ma, K. Guo and S. Fan, *Energy Convers. Manag.*, **44**, 2733 (2003).

Supporting Information

Optimization of water-saturated superabsorbent polymers for hydrate-based gas storage

Min-Kyung Kim*,‡, Geumbi Han*,‡, Hyeonjin Kim*, Jihee Yu*, Youngki Lee*, Taekyong Song, Jinmo Park**, Yo-Han Kim**, and Yun-Ho Ahn*,†**

*Department of Chemical Engineering, Soongsil University, 369 Sangdo-ro, Dongjak-gu, Seoul 06978, Korea
**Hydrogen Research Center, KOGAS Research Institute, 960 Incheonsinhangdaero, Yeonsu-gu, Incheon 21993, Korea
(*Received 12 August 2022 • Revised 18 September 2022 • Accepted 25 September 2022*)

Water-dispersing technique S1: We prepared a desired amount of SAP powders with 30 mL of water based on the targeted WSR value. On the PVC cling film, the SAP powders were spread as thinly as possible, and then 30 mL of water was evenly distributed over the SAP powders. When there was no excess bulk water, the PVC cling film containing water-saturated SAPs was transferred to the reactor. The PVC cling film was attached to the reactor wall to decrease the space between the film and the reactor.

Water-dispersing technique S2: After loading 30 mL of water was loaded into the reactor, tiny amount of SAP powders was slowly added. Once we dropped SAP powders, we waited a few minutes for SAP powders to absorb water entirely.

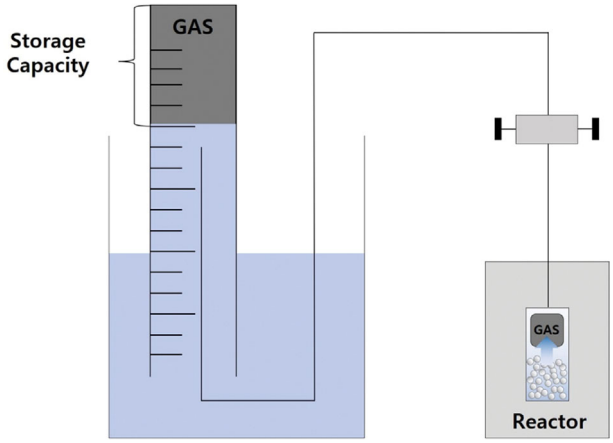

Fig. S1. Schematic diagram of V_{gas}/V_{water} measurement system.

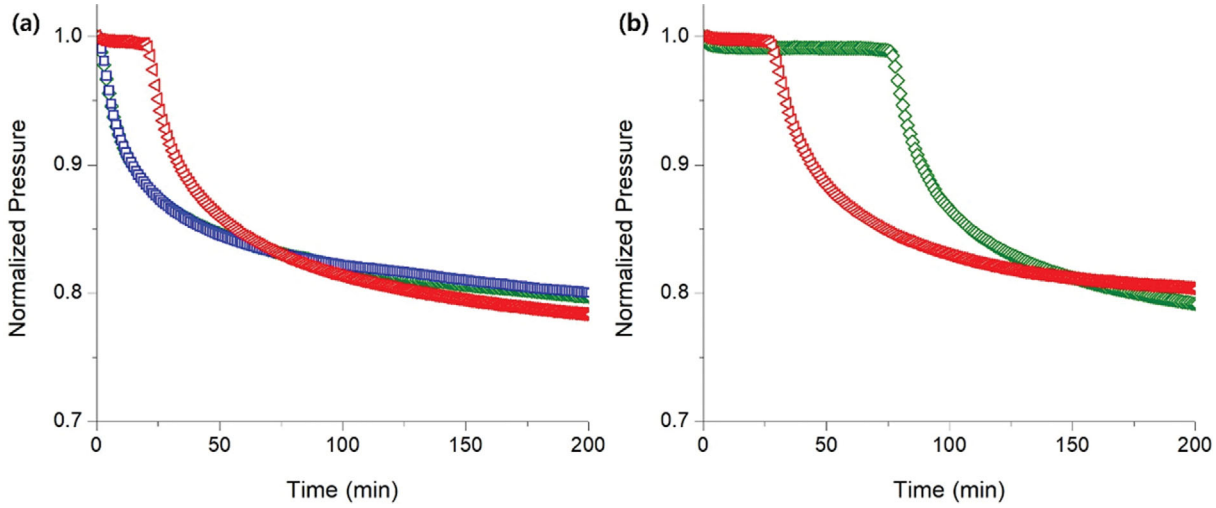

Fig. S2. Kinetic performance at 30 bar (a) in trial 1-2 using water-dispersing technique 1 at WSR 6 (◁, trial 1; ◇, trial 2; □, trial 3) (b) in trial 1-2 using water-dispersing technique 1 at WSR 7 (◁, trial 1; ◇, trial 2).

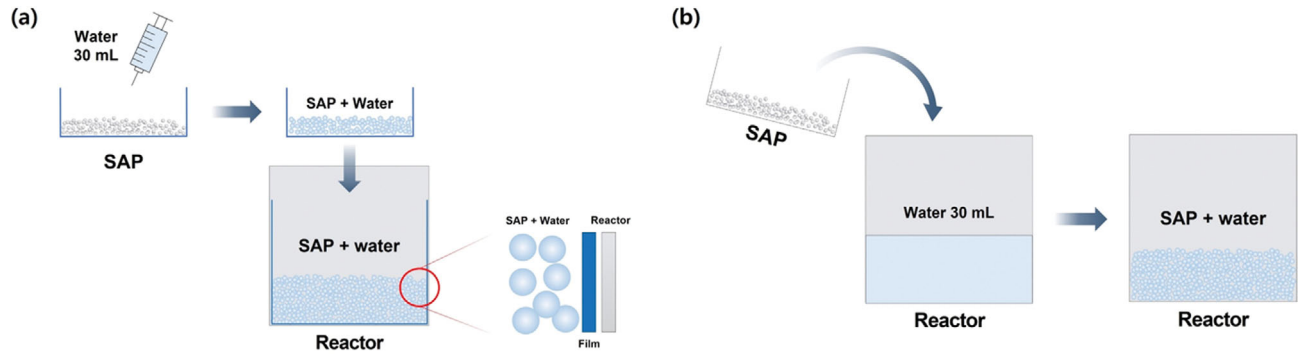

Fig. S3. Schematic diagram of (a) Water-dispersing technique S1, (b) Water-dispersing technique S2.

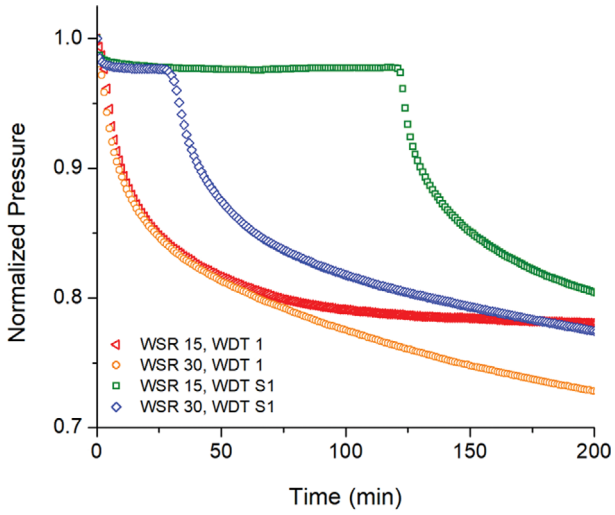

Fig. S4. Pressure changes with $P_{initial}$ of 30 bar for different water-dispersing techniques (WDT) and WSR values (◁, WSR 15, water-dispersing technique 1 (WDT 1); ○, WSR 30, water-dispersing technique 1 (WDT 1); □, WSR 15, water-dispersing technique S1 (WDT S1); ◇, WSR 30, water-dispersing technique S1 (WDT S1)).

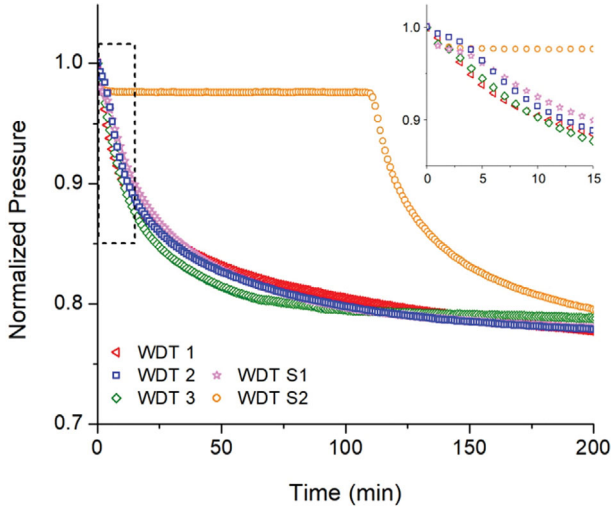

Fig. S5. Pressure changes for various water-dispersing technique with the WSR value of 12 (◁, Water-dispersing technique 1 (WDT 1); □, Water-dispersing technique 2 (WDT 2); ◇, Water-dispersing technique 3 (WDT 3); ☆, Water-dispersing technique S1 (WDT S1); ○, Water-dispersing technique S2 (WDT S2)).

Table S1. Kinetic performances for various water-dispersing techniques with the WSR value of 12 and 54 at 30 bar

Water-dispersing technique	WSR	t_{rapid} [min][a]	$P_{initial}$ [bar]	ΔP [bar][b]	ΔP_{norm} [b]
1	12	103.5833	31.12	6.135	0.1971
2	12	77.083	29.49	5.655	0.1918
3	12	65.583	29.51	5.796	0.1964
1	54	167.333	28.86	5.299	0.1836
2	54	62.333	29.34	4.808	0.1639
3	54	49.083	29.43	5.337	0.1813

[a]The t_{rapid} for WDT 1 with WSR of 54 was the duration time including the induction time. Induction time was 110.25 min.
[b]Time interval of ΔP, ΔP_{norm} was 0~t_{rapid} min.